Interface Stability of Argyrodite Li6PS5Cl toward LiCoO2, LiNi1/3Co1/3Mn1/3O2, and LiMn2O4 in Bulk All-Solid-State Batteries

Jérémie Auvergniot, A. Cassel, Jean-Bernard Ledeuil, V. Viallet, V. Seznec, Rémi Dedryvère

Interface Stability of Argyrodite Li_6PS_5Cl towards $LiCoO_2$, $LiNi_{1/3}Co_{1/3}Mn_{1/3}O_2$ and $LiMn_2O_4$ in Bulk All-Solid-State Batteries

Jérémie Auvergniot [a,b], Alice Cassel [b], Jean-Bernard Ledeuil [a], Virginie Viallet [b,c], Vincent Seznec [b,c,*], Rémi Dedryvère [a,c,*]

[a] IPREM, CNRS UMR 5254, Université de Pau et des Pays de l'Adour
Hélioparc, 2 Avenue Pierre Angot, 64053 Pau Cedex 9, France
[b] LRCS, CNRS UMR 7314, Université de Picardie Jules Verne
33 Rue Saint Leu, 80039 Amiens Cedex, France
[c] Réseau sur le Stockage Electrochimique de l'Energie (RS2E), CNRS FR 3459, France

Abstract

Argyrodite Li_6PS_5Cl is a good candidate as solid electrolyte for bulk all-solid-state Li-ion batteries due to its high ionic conductivity and its good processability. However the interface stability of sulfide-based electrolytes towards active materials (negative or positive electrodes) is known as being lower with respect to oxide-based electrolytes. In the present work we investigate the interface stability of argyrodite towards several positive electrode materials: $LiCoO_2$, $LiNi_{1/3}Co_{1/3}Mn_{1/3}O_2$ and $LiMn_2O_4$. All-solid-state half-cells were cycled and the interface mechanisms were characterized by Auger Electron Spectroscopy (AES) and X-ray Photoelectron Spectroscopy (XPS). We show that Li_6PS_5Cl is oxidized into elemental sulfur, lithium polysulfides, P_2S_x ($x \geq 5$), phosphates and LiCl at the interface with the positive electrode active materials. In spite of this interface reactivity, good capacity retention was observed over 300 cycles. Li_6PS_5Cl shows some reversible electrochemical activity (redox processes) which may contribute to the reversible capacity of the battery.

* Corresponding authors: remi.dedryvere@univ-pau.fr, vincent.seznec@u-picardie.fr

Table of Contents Graphic

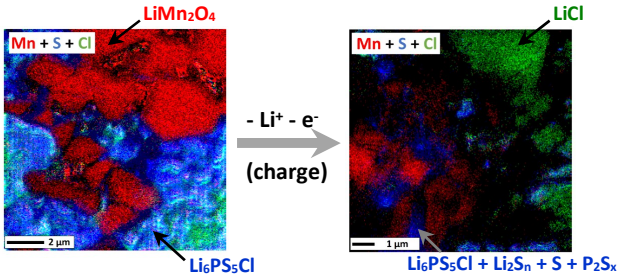

1. Introduction

Lithium-ion batteries are currently the most attractive power sources for mobile electronic devices because they provide high energy density and long cycle life. For some applications, however, the use of an organic liquid electrolyte limits the range of operating temperatures and raises safety issues (risk of leaks, flammability). [1] To solve these issues, bulk « all-solid-state » batteries (ASSB) using an inorganic solid electrolyte are a safer alternative and allow to store more energy than microbatteries. [2,3,4] For good performances, a bulk ASSB needs a very good ionic conductor as solid electrolyte. Argyrodites with general formula $Li_{7-x}PS_{6-x}X_x$ ($0 \leq x \leq 1$, X = Cl, Br, I) are good candidates due to their high Li^+ ion conductivities. [5] Argyrodite Li_6PS_5Cl is an interesting material as solid electrolyte due to its high conductivity ($\sigma = 1.33x10^{-3}$ $S.cm^{-1}$ at 25°C) and its low cost compared to germanium-containing materials such as the well-known $Li_{10}GeP_2S_{12}$. [6,7,8] Li_6PS_5Cl has been therefore studied as solid electrolyte by several groups and has shown promising results in Li-ion and Li-sulfur systems.[9,10,11,12,13,14] However, rapid capacity loss is generally observed, which is suspected to be due to active material/electrolyte interface instability leading to impedance increase. [14]

Interface instability appears indeed as the main scientific issue limiting the development of ASSB. Therefore several theoretical studies have been recently devoted to this issue. [15,16,17] Among interesting solid electrolytes, sulfides show less stable interfaces with active materials than oxides, [15] although they offer better ionic conductivities and better processability. Interestingly, rather few studies have been focused on the chemical characterization of the active material/electrolyte interphases for solid electrolytes with respect to liquid electrolytes. Further investigations are thus necessary to better understand the chemical and electrochemical mechanisms. The characterization of interphases in ASSB offers many advantages compared to liquid electrolyte/electrode interphases. Solid electrolytes are compatible with the ultrahigh vacuum required by many characterization techniques, and the interphases formed with solid electrolytes are less sensitive to electron beams, which allows the use of Auger Electron Spectroscopy.

In the present work, we focus on Li_6PS_5Cl to identify the reasons for capacity fading and to understand the interfacial reactivity between argyrodite and active materials. All-solid-state half cells $LiCoO_2/Li_6PS_5Cl/Li\text{-}In$, $LiNi_{1/3}Co_{1/3}Mn_{1/3}O_2/Li_6PS_5Cl/Li\text{-}In$ and $LiMn_2O_4/Li_6PS_5Cl/Li\text{-}In$ were electrochemically cycled. The composite positive electrodes were analyzed by Auger

Electron Spectroscopy (AES) and X-ray Photoelectron Spectroscopy (XPS), two complementary surface-sensitive characterization techniques.

2. Experimental section

Argyrodite Li_6PS_5Cl was synthesized from Li_2S (Sigma Aldrich 99%), P_2S_5 (Sigma Aldrich 99%) and LiCl (Acros Organic 99%) reagents by ball-milling for 10 h at 600 rpm under argon atmosphere. Argyrodite was used as the solid electrolyte in all-solid state half cells, in which a lithium-indium alloy (6 wt.% of Li) was used as the counter electrode. The composite positive electrodes were formulated using 38% of active material ($LiCoO_2$, $LiNi_{1/3}Co_{1/3}Mn_{1/3}O_2$ or $LiMn_2O_4$), 57% of solid electrolyte Li_6PS_5Cl and 5% of carbon fibers (VGCF) as conducting additive. The components were mixed by grinding in an agate mortar, then pressed at 6.4 tons.cm^{-2}. The resulting composite positive electrode was about 10 mg heavy and 90 µm thick. It was separated from the Li-In electrode by a 570 µm thick electrolyte layer containing only argyrodite. The thickness of the whole half-cell was about 790 µm. The surface loading of active material was 5 mg/cm^2, and the applied current density was 66 µA/cm², corresponding to a C/10 cycling rate (which means that the full charge capacity of the cell is reached in 10 h). The electrochemical measurements where done using the cell described by Boulineau et al. [13] in which the two stainless steel pistons are embedded in a clamp to maintain constant pressure upon cycling.

X-ray Photoelectron Spectroscopy (XPS) was carried out with a Kratos Axis Ultra spectrometer using a focused monochromatized Al Kα radiation (hν = 1486.6 eV). Repeatability of the analysis was systematically tested by using multiple spots on every sample. The non-degradation of the samples under the X-ray beam was checked by recording different spectra of the same sample at different times. The detailed experimental conditions can be found elsewhere. [18]

Auger Electron Spectroscopy (AES) analysis was performed with a JEOL JAMP 9500F Auger Spectrometer (JEOL Ltd, Tokyo, Japan) also used for Scanning Electron Microscopy (SEM). AES spectra were recorded between 50 and 800 eV kinetic energy in constant retarding ratio (CRR) mode with ΔE/E = 0.5% at a working distance of 23 mm, with a 10 kV potential and a 1 nA current. The pressure was lower than 2x10^{-7} Pa. SEM images were obtained with the same machine.

For all analyses, thorough precautions were taken to preserve the samples surface from contact with air and moisture. Batteries were opened in dry argon atmosphere. The XPS introduction chamber was directly connected to the argon glovebox. For AES a vacuum transfer chamber was used.

For Scanning Auger Microscopy (SAM) analysis, the batteries were cross-cut with a JEOL Cross-Polisher (JEOL Ltd, Tokyo, Japan) by the ion-milling polishing method. To this aim, one half of the battery was protected by a stainless steel shield plate and the non-protected area was etched by an Ar^+ ion beam (6 keV). A very clean polished surface was obtained due to the grazing angle (about 2° to the surface) leading to limited implantation of Ar^+ ions in the etched sample.

XPS analysis was carried out at different depths in order to characterize the buried electrode/electrolyte interphases inside the electrodes. First, the positive electrode surface was analyzed as is, *i.e.* the surface that was in contact with the current collector (stainless steel). Then the composite electrode was mechanically scraped with a scalpel blade in the argon glove box (which is directly connected to the XPS machine) in order to remove a 5 μm thick layer of electrode and uncover the active material and argyrodite particles located deeper inside the electrode. This procedure was operated several times to characterize the electrode by XPS at increasing probe depths. The etching depth varied from 5 to 20 μm, meaning that the positive electrode mixture was not etched away completely.

3. Results and discussions

3.1. Electrochemical cycling

$LiCoO_2$, $LiNi_{1/3}Co_{1/3}Mn_{1/3}O_2$ and $LiMn_2O_4$ active materials will be called hereafter LCO, NMC and LMO, respectively. LCO/Li_6PS_5Cl/Li-In half-cells were cycled for 25 cycles between 2.6 and 4.3 V. LMO/Li_6PS_5Cl/Li-In half-cells were cycled for 22 cycles between 2.4 and 4.0 V. NMC/Li_6PS_5Cl/Li-In half-cells were cycled for 300 cycles between 2.8 and 3.4 V. Figure 1 shows the voltage vs. capacity galvanostatic curves, and the capacity retention vs. cycle number for the three cells.

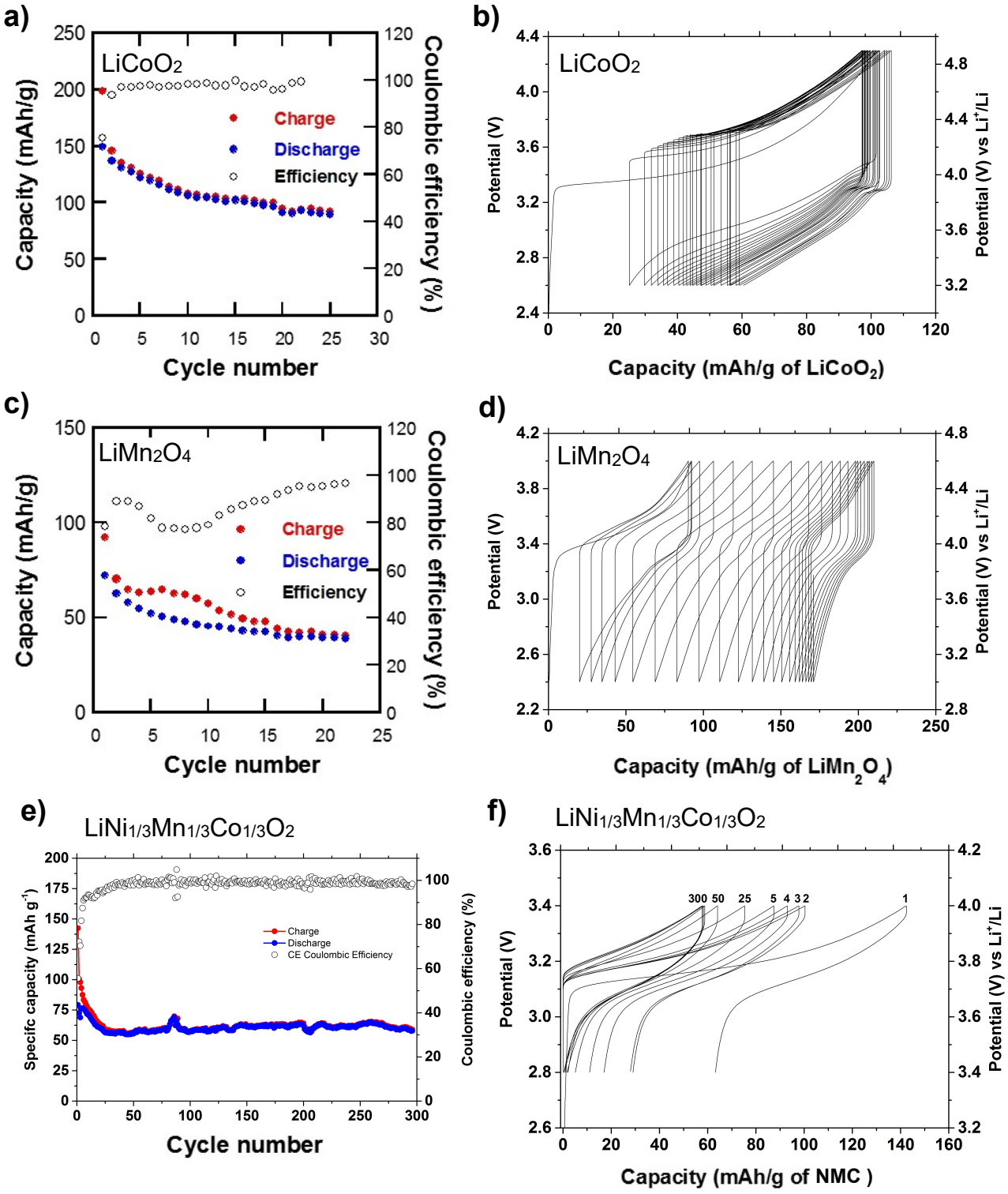

Figure 1: Electrochemical behaviour of LCO / Li_6PS_5Cl /Li-In, LMO / Li_6PS_5Cl /Li-In and NMC / Li_6PS_5Cl / Li-In half-cells: **a)**, **c)**, **e)** Capacity retention vs. cycle number and cycling efficiency. **b)**, **d)**, **f)** Charge-discharge voltage profiles (for NMC only selected cycles are plotted).

For LCO (Figure 1a) the initial discharge capacity is 150 mAh/g then drops to 90 mAh/g after 25 cycles. The coulombic efficiency is rather poor during the first two cycles, then reaches 97% from the third cycle. In the voltage vs. capacity curve (Figure 1b) we can observe a gradual increase of the polarization upon cycling.

For LMO (Figure 1c), after a first discharge capacity of 73 mAh/g, the capacity rapidly decreases to 40 mAh/g after 22 cycles. The coulombic efficiency is much lower than for LCO, it drops down to 80% during the first ten cycles and then re-increases up to 96% after 22 cycles. The voltage vs. capacity curve (Figure 1d) shows no clear evolution of the polarization.

For NMC (Figure 1f) the voltage window was limited to 2.8-3.4 V for long-term cycling so the initial discharge capacity was only 80 mAh/g. After a capacity fading down to 60 mAh/g over the first 20 cycles, the discharge capacity stabilized and no additional capacity fading was observed for 300 cycles.

The aim of the following part of the paper is to carry out the chemical characterization of the interphases between argyrodite and the active materials after cycling. We investigated the composite positive electrodes for the three different active materials LCO, LMO and NMC.

3.2. Study of LCO and LMO electrodes after 22-25 cycles

The composite electrodes contain active material particles but also argyrodite particles and carbon fibers. The structure of the all-solid-state half-cells is shown in Figure 2. The positive electrode actually contains more solid electrolyte than active material (57 vs. 38%) to allow Li^+ ions from the electrolyte to reach all the active material particles inside the electrode (*i.e.* what is called wettability of the electrode for a liquid electrolyte). The part of the battery called « electrolyte » only consists of argyrodite particles. The limit between the positive electrode and the electrolyte is found where no more active material particles are present.

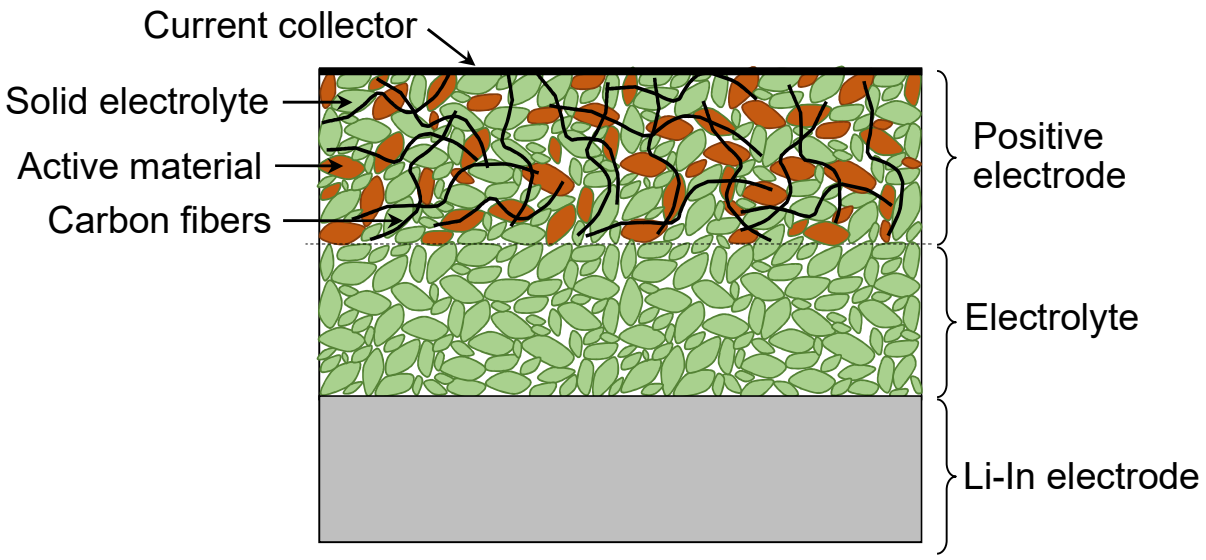

Figure 2: Schematic view of a cross-section of the all-solid-state half cells studied in this work

3.2.1. XPS study of LCO/argyrodite interface

The S 2p and P 2p XPS spectra of argyrodite in the LCO composite electrode before (pristine) and after 25 cycles are shown in Figure 3. S 2p and P 2p signals are split in two components due to spin-orbit coupling, with an area ratio of about 2/1. Each chemical environment of S or P corresponds to one $2p_{3/2}$-$2p_{1/2}$ doublet.

The S 2p spectrum of the pristine electrode shows a main doublet with S $2p_{3/2}$ component at a binding energy (BE) of 161.7 eV (red component) attributed to the sulfur atoms of argyrodite. An additional weak doublet at 160.5 eV (gray component) can be attributed to Li_2S and corresponds to remaining traces of this reagent used for the synthesis (this was also confirmed by X-ray diffraction data, see Figure S1 in supporting information). A third weak component at 167.1 eV can be hardly detected. It is explained by traces of sulfite environment (SO_3^{2-}) at the surface, probably due to contact with traces of oxygen. Note that XPS spectra of the pristine Li_6PS_5Cl powder (Figure S2 in supporting information) were exactly the same as in the uncycled electrode.

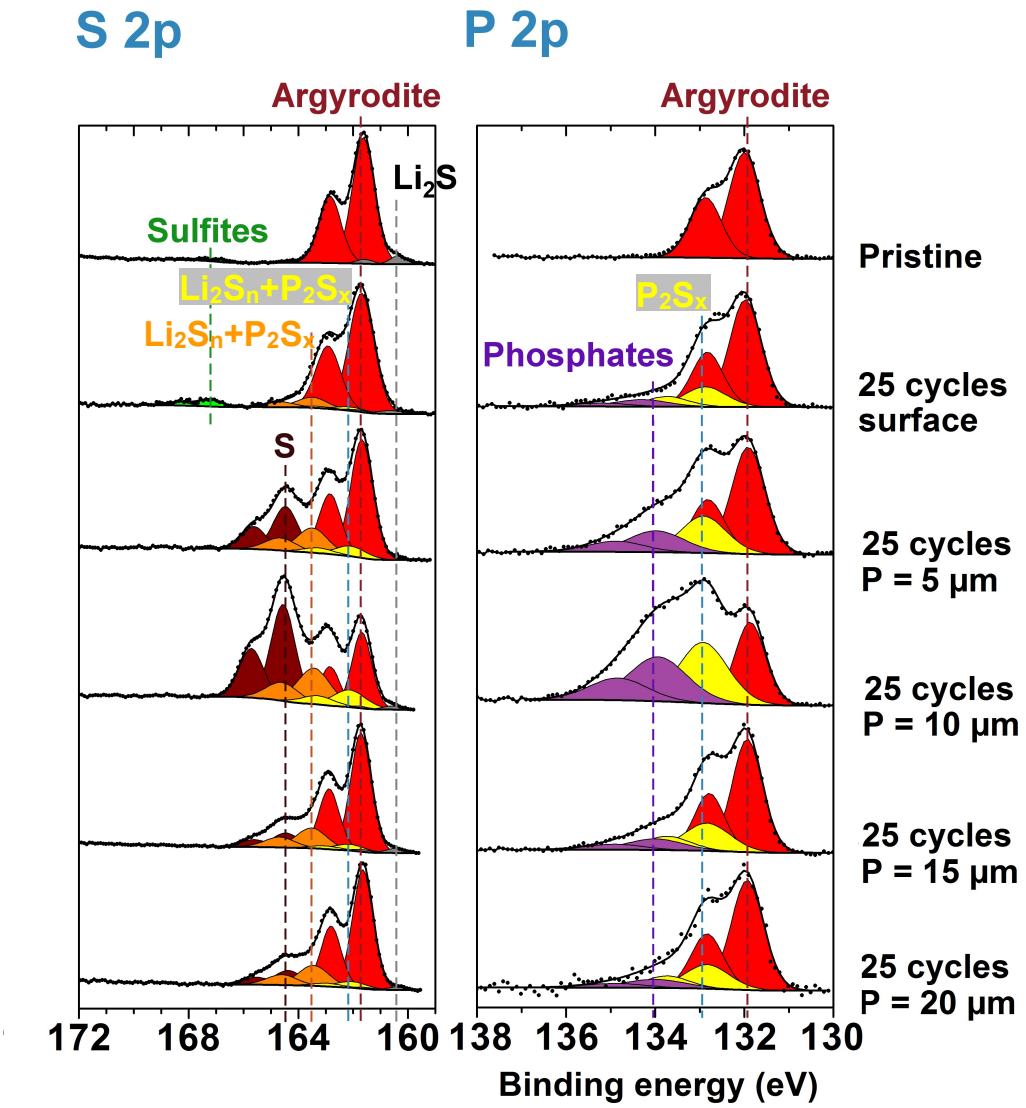

Figure 3: S 2p and P 2p XPS spectra of the composite LCO electrode of LCO/Li_6PS_5Cl/Li-In half-cells: before cycling (pristine), after 25 cycles, and after 25 cycles with increasing etching depths of the electrode from 5 to 20 µm.

After 25 cycles the S 2p spectrum of the electrode surface is modified. The S 2p signal of Li_2S decreases whereas the signal of sulfites increases. Moreover an additional doublet (S $2p_{3/2}$ at BE = 163.5 eV, orange in Figure 3) was necessary to fit correctly the spectrum. Etching a 5 or 10 µm thick layer from the electrode surface resulted in an intensity increase of this new sulfur environment, together with the disappearance of the sulfite and the appearance of other sulfur environments. An S 2p doublet at BE = 164.4 eV (brown

component) appeared, the intensity of which was increasing with etching depth. The BE of this component allowed us to assign it to elemental sulfur. We can thus conclude that argyrodite is oxidized into elemental sulfur within the positive electrode. Taking into account that the Li_2S signal decreased with respect to the pristine electrode, the appearance of elemental sulfur may also be partly due to the oxidation of Li_2S. This is indeed the oxidation mechanism usually observed during the charge of a lithium-sulfur (Li-S) battery. [19] However, the amount of Li_2S in the pristine electrode was too small to explain the amount of elemental sulfur observed after 25 cycles. Therefore an oxidation process of the argyrodite itself occurs, probably because it is in electronic contact with the charged LCO active material.

When the electrode surface was mechanically etched after 25 cycles, a last additional S 2p component was necessary to fit correctly the spectrum (S $2p_{3/2}$ at BE = 162.1 eV, yellow component). The simultaneous presence of two components at BE = 163.5 eV and 162.1 eV (orange and yellow, respectively) is perfectly consistent with the presence of lithium polysulfides Li_2S_n, since these two BE are those observed for bridging and terminal sulfur atoms of polysulfides, respectively. [20] It is worth noting that lithium polysulfides are also produced in Li-S batteries by oxidation of Li_2S upon charge, or by reduction of elemental sulfur upon discharge. In our case, the presence of Li_2S_n species may be due either to the reduction of elemental sulfur, or by direct oxidation of argyrodite. The two S 2p components at BE = 163.5 eV and 162.1 eV are also in good agreement with the formation of P_2S_x species ($x > 5$) containing S-...-S chains, as explained later.

The intensity of these new S 2p components is strongly dependent on the etching depth, especially concerning the elemental sulfur. Its intensity is maximum for an etching depth of 10 μm. It drops significantly after etching a 15 μm thick layer of the surface, and then it remains constant after deeper etching (20 μm). These results show that electrochemical mechanisms are not homogeneous in the whole electrode, and depend on the distance to the current collector.

Concerning P 2p spectra, the signature of argyrodite consists of a doublet at BE $2p_{3/2}$ = 132.0 eV and is the only component observed in the pristine electrode. Additional components are observed after 25 cycles. The first one at BE = 133.0 eV (yellow in Figure 3) is in good agreement with the XPS signature of P_2S_5 reported by other authors,[21] which was confirmed by an internal P_2S_5 reference in the lab. Note that the formation of P_4S_{10}

molecules by oxidation of Li_6PS_5Cl is unlikely. A disordered «P_2S_5» compound containing bridging and terminal sulfur atoms can be formed. The presence of P_2S_5 is also in good agreement with S 2p spectra because the two different environments of sulfur atoms in P_2S_5 , *i.e.* the terminal sulfur (P=S groups) and the bridging sulfur (P-S-P groups) overlap with S 2p components of polysulfides Li_2S_n at 162.1 and 163.5 eV, respectively. However the measured P 2p peak intensity of P_2S_5 is too weak to explain the whole S 2p intensity (P/S ratio), therefore a mixture of P_2S_5 and polysulfides should be present in the electrode after 25 cycles, and we can also envisage the formation of P_2S_x species (x > 5) containing P(+V) and S-S bonds with various S-...-S chain lengths. For example, P_2S_7 contains a three-sulfur S-S-S chain as well as the sulfur environments found in P_2S_5 and was already described by other authors.[22] Therefore sulfur can form polysulfides by oxidation of Li_6PS_5Cl, but so does phosphorus through S-...-S chains in P_2S_x species.

An additional P 2p component at higher BE (134.0 eV, violet in Figure 3) was observed, which can be assigned to phosphorus atoms in a more oxidized environment (phosphates). One could think that the presence of phosphates might be due to contact with air during cycling. However, the formation of phosphates is disconnected from the formation of sulfites. Sulfites are present at the surface of the electrode before etching but disappear after removing a 5 μm layer from the surface. On the contrary, phosphates are not present at the surface of the electrode and appear when the surface is mechanically etched. Actually the intensity of phosphate P 2p component follows exactly the same evolution as that of elemental sulfur in S 2p spectra. Therefore the presence of phosphates is due to an electrochemical process in the positive electrode during charge. It could be due to interfacial reactivity of argyrodite towards the charged LCO active material. Indeed, the reactivity of LCO towards a sulfur-based solid electrolyte was already reported by Sakuda *et al*. [23,24] who observed by EDX the diffusion of Co, S and P elements at the interface between LCO and Li_2S-P_2S_5. Moreover, the formation of phosphates at the interface between $LiNi_{0.8}Co_{0.15}Al_{0.05}O_2$ (NCA) and Li_2S-P_2S_5 was already evidenced by Time-of-Flight Secondary Ion Mass Spectrometry (ToF-SIMS) after cycling. [25] Therefore we assume that in our case the presence of phosphates results from the interfacial reaction between Li_6PS_5Cl and the charged LCO.

The heterogeneity of interfacial reactions involving argyrodite within the composite positive electrode is an interesting result. The formation of elemental sulfur, polysulfides,

P_2S_x and phosphates is dependent on the depth, *i.e.* on the distance to the current collector. After 25 cycles these oxidation reactions reach a maximum at about 10 μm depth. As shown recently by Tang et al., [26] the gradient of lithiation (or delithiation) within the electrode depends on two kinetically limiting factors: if the ionic transport within the electrode is the limiting factor, the lithiation (or delithiation) is faster close to the separator than close to the current collector. If electronic conduction is the limiting factor, the lithiation (or delithiation) is faster near the current collector. In our case, the maximum delithiation of Li_6PS_5Cl is observed close to the current collector, but at a distance of 10 μm from it (the thickness of the positive electrode is 90 μm). This means that electron conduction (insured by the carbon additive) is the main limiting factor in our positive electrode. However, close to the current collector, the ionic transport becomes the limiting factor, certainly because chemical changes undergone by the solid electrolyte in the region 10 μm far from the current collector have affected its ionic conductivity. This non uniform distribution of oxidation reactions in the electrode is certainly related to the capacity fading.

Additional information was provided by Li 1s spectra, as shown in Figure 4. The Li 1s spectrum of the pristine electrode is dominated by the Li 1s signal from argyrodite (55.6 eV) because the proportion of solid electrolyte is 57 wt.% in the composite electrode. After 25 cycles, an additional Li 1s component at BE = 56.4 eV was observed, which is in good agreement with the BE reported for LiCl [27] and was confirmed in this work by an experimental LiCl reference. The proportion of LiCl increased after etching 5 or 10 μm of the electrode surface, and decreased after a deeper etching of 15 or 20 μm, which shows again that oxidation reactions are not uniformly distributed within the electrode.

Finally, from our experimental results we can propose an oxidation mechanism of Li_6PS_5Cl into elemental sulfur, polysulfides, P_2S_x species and LiCl, with also the formation of phosphates at the interface with LCO. Note that the anodic stability of solid electrolytes was previously discussed by theoretical studies. By DFT-GGA calculations, Richards *et al.* predicted the oxidation of argyrodite Li_6PS_5Cl into S, P_2S_7 and LiCl. [15] In our case, the formation of elemental sulfur and LiCl is in good agreement with this study.

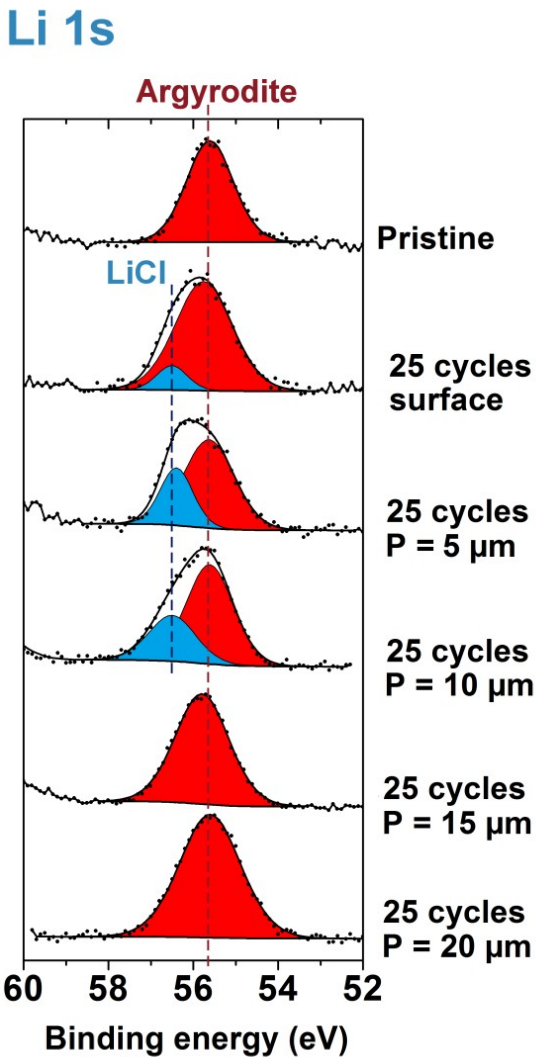

Figure 4: Li 1s spectra of the composite LCO electrode of LCO/Li_6PS_5Cl/Li-In half-cells: before cycling (pristine), after 25 cycles, and after 25 cycles with increasing etching depths of the electrode from 5 to 20 µm.

3.2.2. XPS study of LMO/argyrodite interface

The S 2p and P 2p XPS spectra of argyrodite in the LMO composite electrode before and after cycling are shown in Figure 5. Overall, the same observations could be done, with some important differences. First, the S 2p signature of polysulfides and the P 2p signature of P_2S_x were already seen in the pristine composite electrode. This means that the LMO/argyrodite interface is not stable, even before the beginning of the electrochemical charge or discharge. Therefore the reactivity of argyrodite towards LMO is greater than towards LCO.

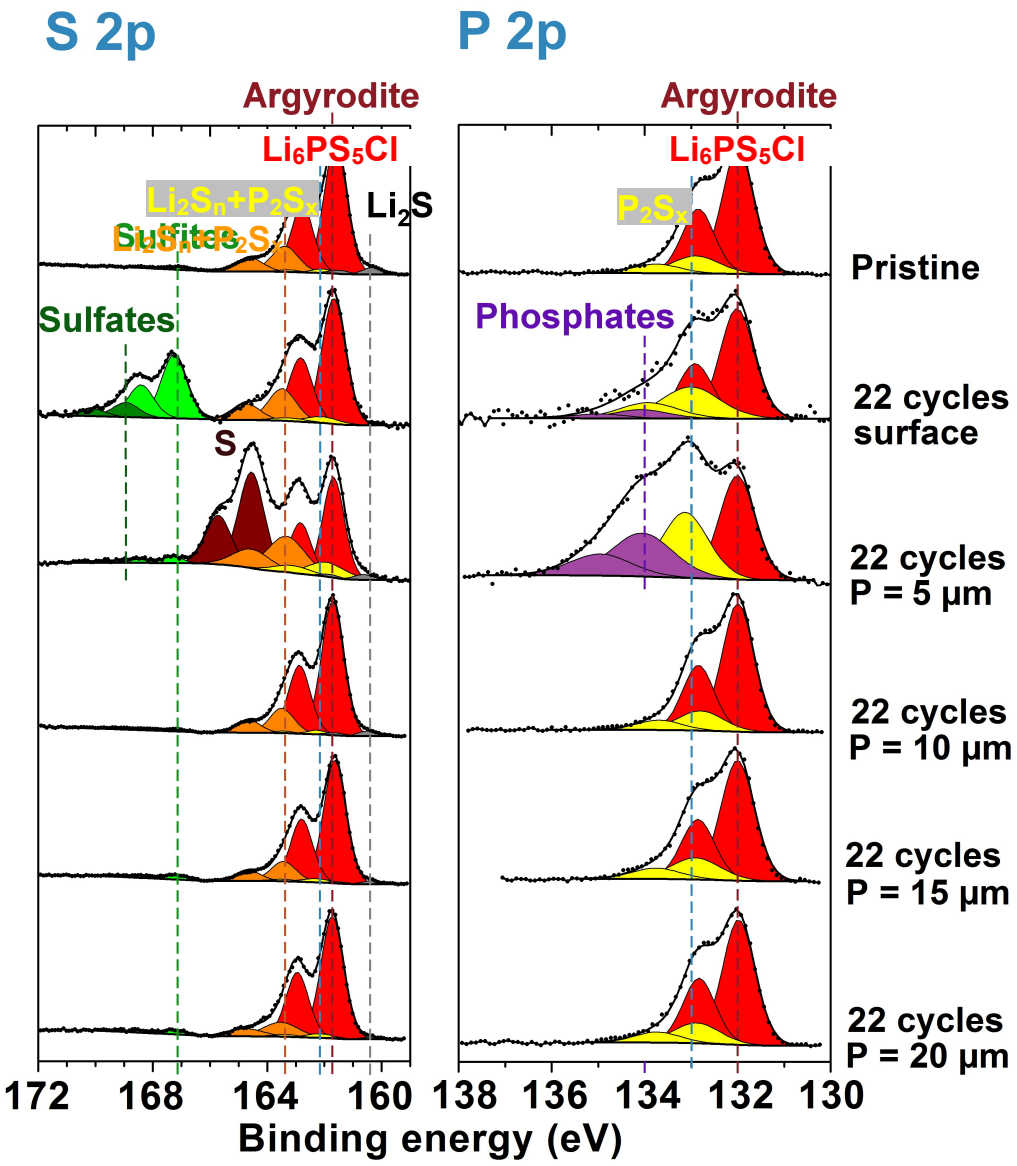

Figure 5: S 2p and P 2p XPS spectra of the composite LMO electrode of LMO/Li_6PS_5Cl/Li-In half-cells: before cycling (pristine), after 22 cycles, and after 22 cycles with increasing etching depths of the electrode from 5 to 20 µm.

After 22 cycles the S 2p spectrum of the LMO electrode surface showed a greater amount of oxidized sulfur species compared to the LCO electrode, with the presence of sulfites and also sulfates. This is certainly the result of oxidation by oxygen from air and may be due to the experimental setup, since these components disappear after mechanical etching.

After etching 5 μm of the LMO electrode's surface, the results obtained in S 2p and P 2p spectra were very similar to those obtained for the LCO electrode after 10 μm etching. Elemental sulfur, polysulfides, P_2S_x species and phosphates were observed in similar relative amounts. However, the dependence of interfacial reactions on the distance to the current collector was very different. The maximum was reached for an etching depth of 5 μm. Deeper etching resulted in the disappearance of elemental sulfur and phosphates. As a result, S 2p and P 2p spectra obtained for etching depths greater than 10 μm were similar to the pristine LMO electrode, as though there was no electrochemical activity in the deeper parts of the electrode. This confirms that the heterogeneity of interfacial reactions within the electrode may be linked to the capacity fading and to a loss of electronic percolation upon cycling, since the electrochemical performances of the LMO electrode were much worse than those of LCO electrode.

3.2.3. Auger electron imaging of $LiMn_2O_4$ electrode

The chemical characterization carried out by XPS was complemented by Scanning Auger Microscopy (SAM) analysis. The main advantage of Auger electron spectroscopy is its very good lateral resolution compared to XPS, although it does not allow the same possibilities for chemical characterization. SAM analysis was carried out on a cross-section of the LMO electrode before (pristine) and after 22 cycles in order to map characteristic elements and detect any changes in their location in the electrode. A clean cross-section was achieved by a specific cross polisher (see experimental section). Figure 6 shows the Mn LMM, S LVV and Cl LVV SAM images of the LMO pristine electrode, together with its Scanning Electron Microscopy (SEM) image. The Mn LMM image allows to clearly identify the cross-cut LMO particles. On the other hand, the S LVV and Cl LVV images allow the identification of Li_6PS_5Cl particles. It is worth noting that the S and Cl signals perfectly overlap, since these elements are found only in argyrodite and not in LMO. The minima observed for Mn signal roughly correspond to the maxima of S and Cl signals, and so the S and Cl images are a negative of the Mn image.

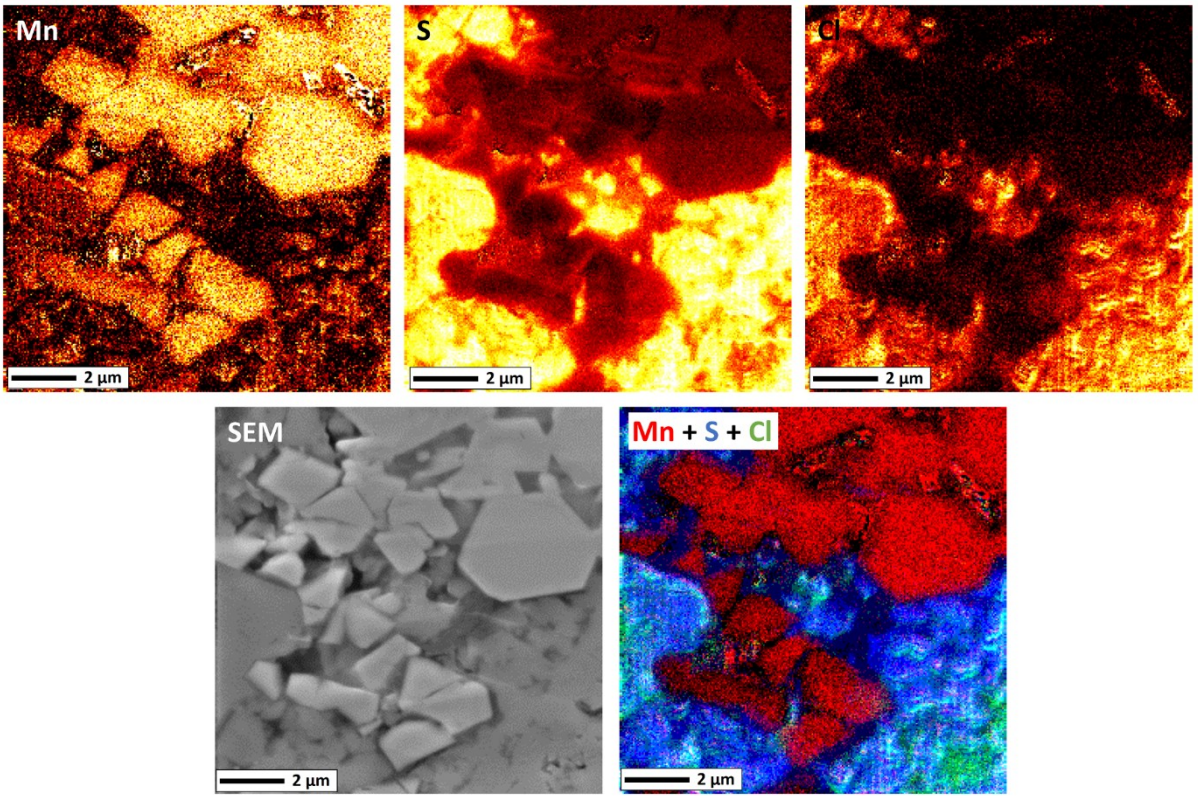

Figure 6: SEM image and SAM mapping of Mn, S and Cl elements from a cross-section of the composite LMO electrode of LMO/Li_6PS_5Cl/Li-In half-cell before cycling (pristine) (Bar = 2 µm)

The same kind of analysis was carried out on the LMO electrode after 22 cycles. It is shown in Figure 7. Mn and S images still remain complementary, *i.e.* the minima of Mn signal correspond to the maxima of S signal. There is thus a clear distinction between the particles containing manganese (LMO particles) and the particles containing sulfur. The results are very different when it comes to S and Cl images. Indeed, there is no clear correspondence between S and Cl Auger signals, in such a way that sulfur-rich particles seem to be partially disconnected from chlorine-rich particles. This is in good agreement with the results of XPS characterization, which allowed us to conclude that Li_6PS_5Cl is oxidized into sulfur-containing species (S, Li_2S_n, P_2S_x) and LiCl. Therefore the SAM imaging of the electrode allows us to evidence the spatial separation between LiCl particles (probably crystalline) and other sulfur-containing particles.

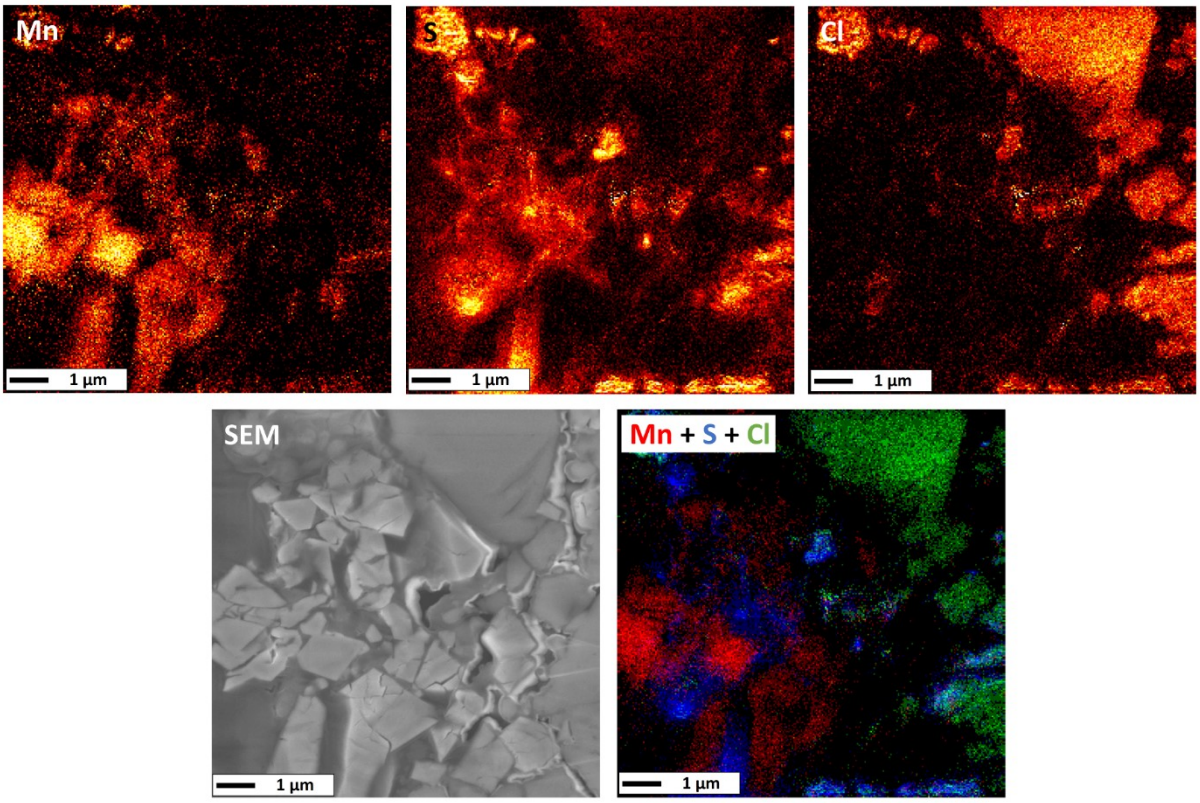

Figure 7: SEM image and SAM mapping of Mn, S and Cl elements from a cross-section of the composite LMO electrode of LMO/Li_6PS_5Cl/Li-In half-cell after 22 cycles. (Bar = 1 µm)

3.3. Study of NMC electrode after 300 cycles

This study was complemented by the analysis of the argyrodite/NMC active material interface after a much longer cycling, *i.e.* after 300 cycles. Figure 8 shows the S 2p and P 2p XPS spectra of argyrodite in the pristine NMC composite electrode, after the first charge, after 1 cycle, and after 300 cycles. The composite electrode recovered after 300 cycles was analyzed before and after etching 5 µm of its surface, as done before for LCO and LMO electrodes.

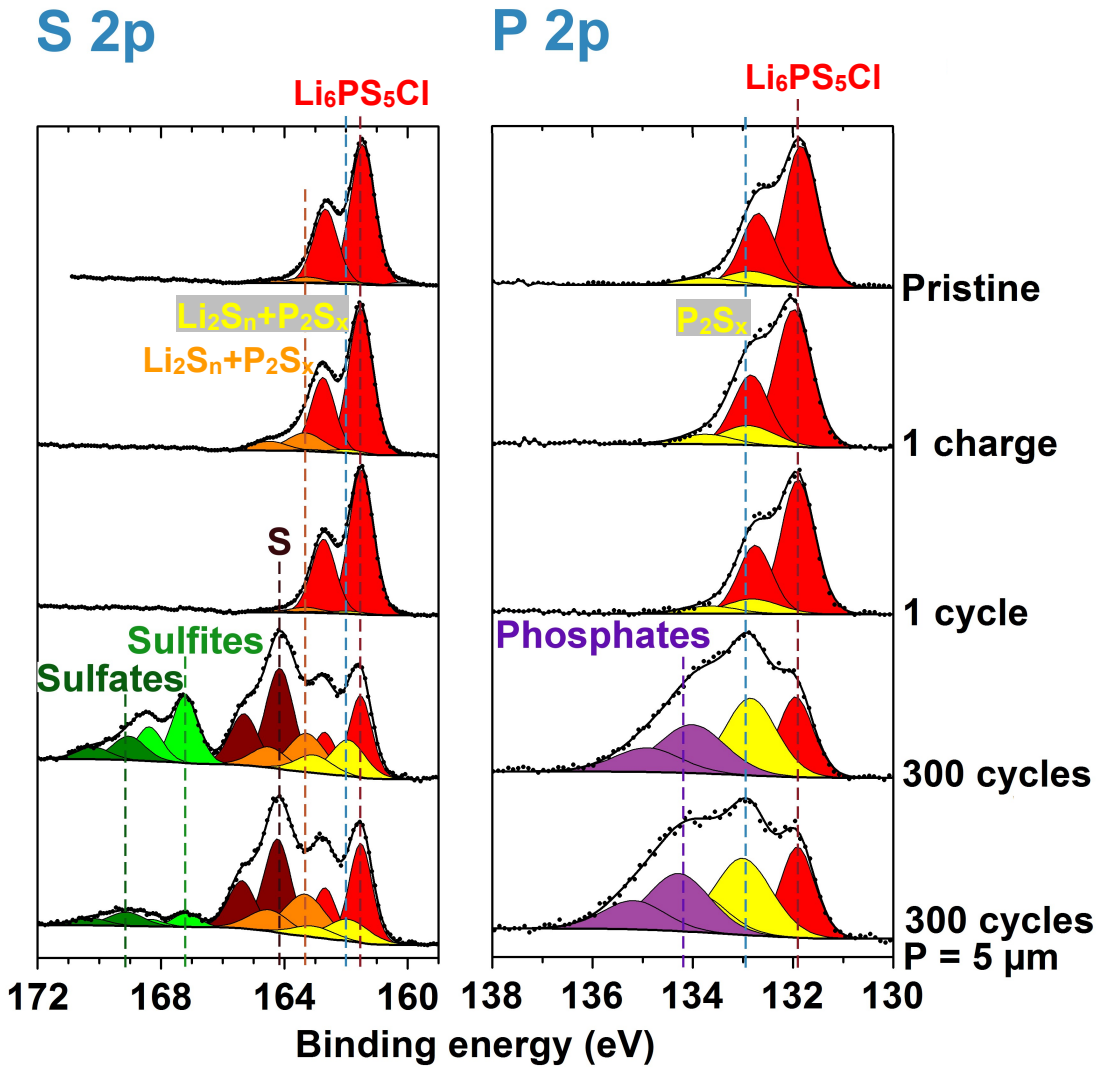

Figure 8: S 2p and P 2p spectra of the composite NMC electrode of NMC/Li_6PS_5Cl/Li-In half-cells: before cycling (pristine), after the 1st charge, after 1 cycle, and after 300 cycles with and without etching 5 µm of the electrode surface.

There was almost no difference observed between the pristine electrode and after 1 cycle. Therefore no significant oxidation of argyrodite could be evidenced. However, after the first charge the polysulfides S 2p component at 163.5 eV was more intense than after a full cycle. As a comparison, it was greater than in the LCO electrode after 25 cycles, as shown previously in Figure 3. Therefore the oxidation process of argyrodite occurs upon charge and is partially reversible upon discharge. Progressive accumulation of oxidation products of argyrodite can be observed after repeated cycles.

It is worth noting that a weak polysulfide S 2p component could be already detected in the pristine NMC electrode, which means that the NMC/argyrodite interface is slightly less stable than the LCO/argyrodite interface. However, the presence of oxidation species of argyrodite was much lower than with LMO. Therefore from our experiments we can propose that the chemical reactivity of argyrodite towards these three active materials follows the ranking LCO < NMC << LMO. Note that LCO and LMO materials have been in contact for two weeks with the solid electrolyte in the pristine electrode before XPS analysis (for NMC: three weeks). Therefore the differences of reactivity towards Li_6PS_5Cl observed between the active materials cannot be attributed to kinetics. Interestingly, the open-circuit voltages of the half-cells measured after 10h relaxation before starting the cycling were 1.78, 1.75 and 2.32 V vs. Li-In for LCO, NMC and LMO, respectively. Therefore, the greater reactivity of LMO with respect to the two layered oxides could be due to its greater potential.

After long-term cycling (300 cycles) the same observations could be made in S 2p and P 2p spectra as for LCO and LMO electrodes after 22 and 25 cycles. Indeed elemental sulfur, polysulfides, P_2S_x and phosphates could be detected at the NMC composite electrode surface after 300 cycles. The main difference was that elemental sulfur and phosphates were detected at the surface without any etching of the surface, whereas it was necessary to etch at least 5 µm of the LCO and LMO composite electrodes to let these species appear. Interestingly, after etching 5 µm of the NMC electrode surface the amounts of S, Li_2S_n, P_2S_x and PO_4 did not significantly change, contrary to what was observed with the LCO and LMO electrodes. Instead, only the amount of sulfites and sulfates decreased, which confirms that these species are due to oxidation by oxygen from air, whereas the other detected species (including phosphates) result from interface reactivity between argyrodite and the active material.

Finally we can observe that, although argyrodite decomposes into several oxidation products at interfaces, the NMC/argyrodite/Li-In half-cell displays a very good capacity retention over 300 cycles (after an initial loss during the first 20 cycles). Therefore the interface reactivity of argyrodite toward active materials and toward oxidation authorizes its use as solid electrolyte. The partial reversibility of oxidation processes of this electrolyte between charge and discharge, as shown in Figure 8, might even contribute to the reversible capacity of the battery. Interestingly, previous papers have reported the electrochemical activity of several solid electrolytes. Han *et al.* showed the possibility of cycling a full cell

made from $Li_{10}GeP_2S_{12}$ as one single material playing the roles of cathode, anode and solid electrolyte. [28] Tarhouchi *et al.* reported the electrochemical cycling of batteries using $Li_{10}SnP_2S_{12}$ as both negative electrode and solid electrolyte. [29]

4. Conclusion

In this paper we have investigated the interface reactivity of Li_6PS_5Cl towards the three active materials LCO, NMC and LMO upon cycling. We have shown by XPS that argyrodite is oxidized into elemental sulfur, lithium polysulfides, P_2S_x ($x \geq 5$), phosphates and LiCl at the interface with the positive electrode active material. SAM imaging revealed the separation between LiCl particles and sulfur-containing particles. Interestingly, these oxidation processes of the electrolyte do not hinder the good cyclability of the battery since a good capacity retention was observed over 300 cycles for the NMC/argyrodite/Li-In half-cell (after an initial loss during the first 20 cycles). Moreover, the partial reversibility of the oxidation processes of argyrodite (reversible formation of elemental sulfur and polysulfides) shows the electrochemical activity of argyrodite which behaves not only as an electrolyte but also may contribute to the reversible capacity of the composite electrode.

Acknowledgments:

The authors thank the French National Research Agency (ANR) for financial support of Labex STORE-EX (ANR-10-LABX-0076).

Supporting Information

X-ray diffraction pattern (figure S1) and S 2p and P 2p XPS spectra (figure S2) of the pristine argyrodite material.

Supporting information

Interface Stability of Argyrodite Li_6PS_5Cl towards $LiCoO_2$, $LiNi_{1/3}Co_{1/3}Mn_{1/3}O_2$ and $LiMn_2O_4$ in Bulk All-Solid-State Batteries

Jérémie Auvergniot [a,b], Alice Cassel [b], Jean-Bernard Ledeuil [a], Virginie Viallet [b,c], Vincent Seznec [b,c,*], Rémi Dedryvère [a,c,*]

[a] IPREM, CNRS UMR 5254, Université de Pau et des Pays de l'Adour
Hélioparc, 2 Avenue Pierre Angot, 64053 Pau Cedex 9, France
[b] LRCS, CNRS UMR 7314, Université de Picardie Jules Verne
33 Rue Saint Leu, 80039 Amiens Cedex, France
[c] Réseau sur le Stockage Electrochimique de l'Energie (RS2E), CNRS FR 3459, France

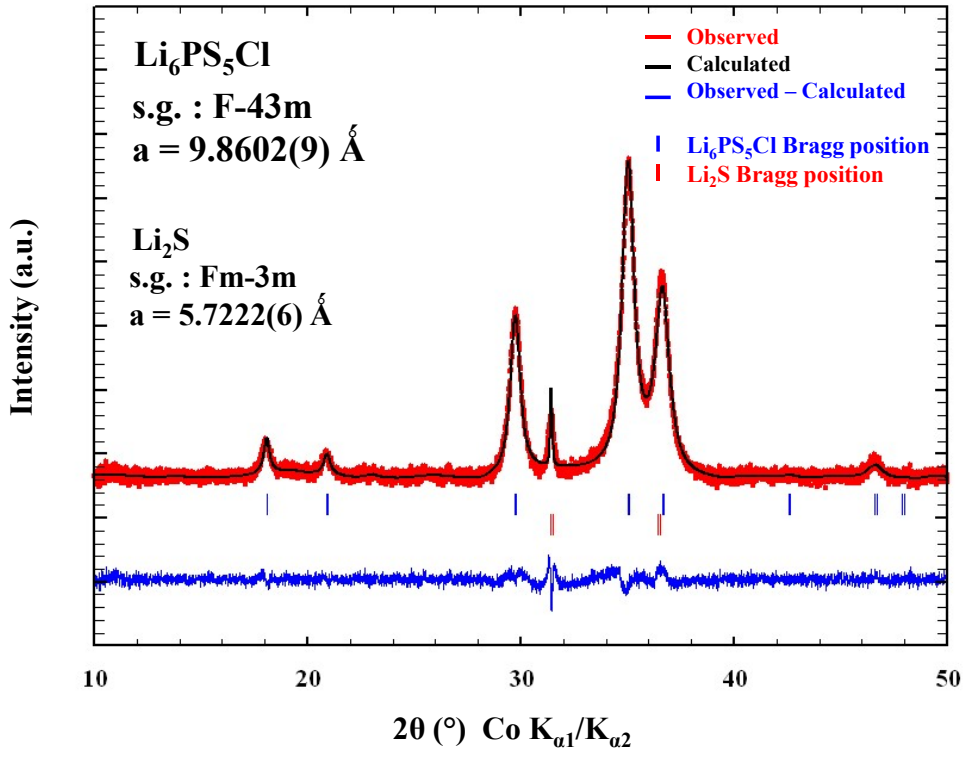

Figure S1: X-ray diffraction pattern of the pristine Li_6PS_5Cl. material used in this work. Rietveld refinement showing the presence of a small amount of crystalline Li_2S mixed with Li_6PS_5Cl.

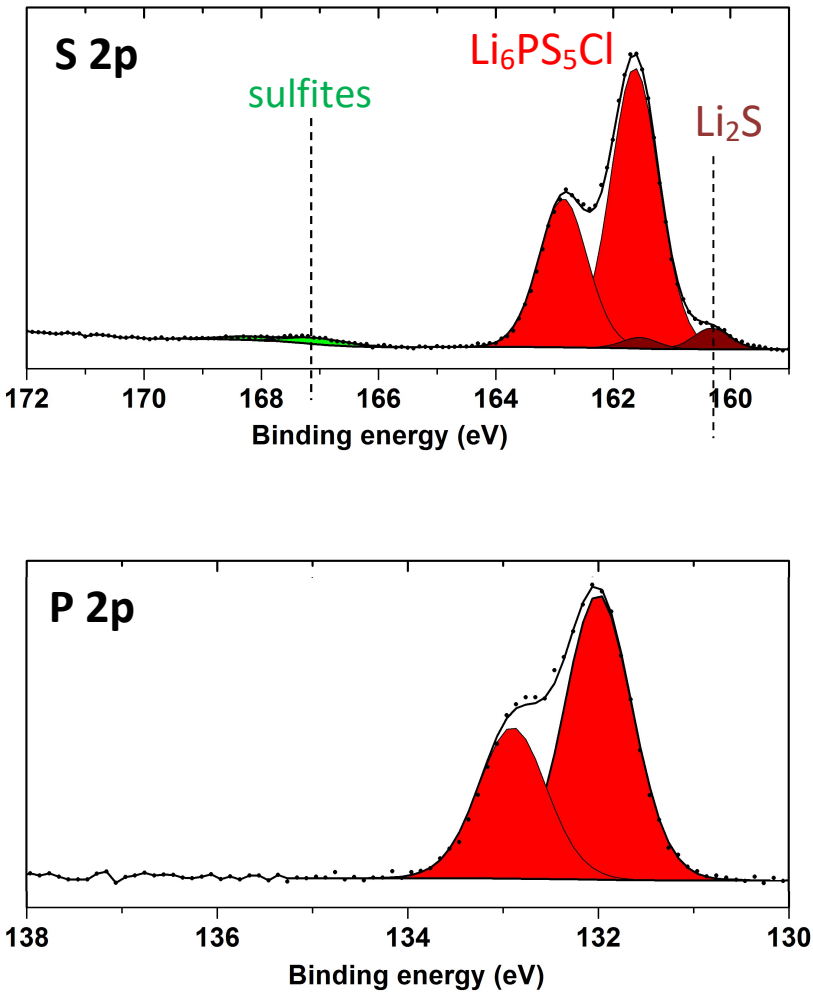

Figure S2: S 2p and P 2p XPS spectra of the pristine Li_6PS_5Cl powder.

References

[1] Boulineau, S.; Courty, M.; Tarascon, J.-M.; Viallet, V.; Mechanochemical Synthesis of Li-Argyrodite Li_6PS_5X (X = Cl, Br, I) as Sulfur-based Solid Electrolytes for All Solid State Batteries Application; *Solid State Ionics* **2012**, *221*, 1–5

[2] Birke, P.; Salam, F.; Döring, S.; Weppner, W.; A First Approach to a Monolithic All Solid State Inorganic Lithium Battery; *Solid State Ionics* **1999**, *118*, 149–157

[3] Aboulaich, A.; Bouchet, R.; Delaizir, G.; Seznec, V.; Tortet, L.; Morcrette, M.; Rozier, P.; Tarascon, J.-M.; Viallet, V.; Dollé, M.; A New Approach to Develop Safe All-Inorganic Monolithic Li-Ion Batteries; *Adv. Energy Mater.* **2011**, *1* (2), 179–183

[4] Masquelier, C.; Solid Electrolytes: Lithium Ions on the Fast Track; *Nat. Mater.* **2011**, *10* (9), 649–650

[5] Deiseroth, H.-J.; Kong, S.-T.; Eckert, H.; Vannahme, J.; Reiner, C.; Zaiss, T.; Schlosser, M.; Li_6PS_5X: A Class of Crystalline Li-Rich Solids with an Unusually High Li^+ Mobility; Angew. Chem. 2008, 47, 755–758.

[6] Kamaya, N; Homma, K.; Yamakawa, Y.; Hirayama, M.; Kanno, R.; Yonemura, M.; Kamiyama, T.; Kato, Y.; Hama, S.; Kawamoto, K.; Mitsui, A.; A Lithium Superionic Conductor; *Nat. Mater.*, 2011, **10**(9), 682-686

[7] Pecher, O.; Kong, S. T.; Goebel, T.; Nickel, V.; Weichert, K.; Reiner, C.; Deiseroth, H. J.; Maier, J.; Haarmann, F.; Zahn, D.; Atomistic Characterisation of Li^+ Mobility and Conductivity in $Li_{7-x}PS_{6-x}Ix$ Argyrodites from Molecular Dynamics Simulations, Solid-State NMR, and Impedance Spectroscopy; *Chem. Eur. J.* **2010**, *16* (28), 8349–8354

[8] Rao, R. P.; Adams, S.; Studies of Lithium Argyrodite Solid Electrolytes for All-Solid-State Batteries; *Phys. Status Solidi* **2011**, *208* (8), 1804–1807

[9] Chen, M.; Prasada Rao, R.; Adams, S.; The Unusual Role of Li_6PS_5Br in All-Solid-State CuS/Li_6PS_5Br/In-Li Batteries; *Solid State Ionics* **2014**, *268* (PB), 300–304

[10] Chen, M.; Adams, S.; High Performance All-Solid-State Lithium/Sulfur Batteries Using Lithium Argyrodite Electrolyte; *J. Solid State Electrochem.* **2015**, *19*, 697–702

[11] Chen, M.; Rao, R. P.; Adams, S.; High Capacity All-Solid-State Cu-Li_2S/Li_6PS_5Br/In Batteries; *Solid State Ionics* **2014**, *262*, 183–187

[12] Yubuchi, S.; Teragawa, S.; Aso, K.; Tadanaga, K.; Hayashi, A.; Tatsumisago, M.; Preparation of High Lithium-Ion Conducting Li_6PS_5Cl Solid Electrolyte from Ethanol Solution for All-Solid-State Lithium Batteries; *J. Power Sources* **2015**, *293*, 941–945

[13] Boulineau, S.; Tarascon, J.-M.; Leriche, J.-B.; Viallet, V.; Electrochemical Properties of All-Solid-State Lithium Secondary Batteries Using Li-Argyrodite Li_6PS_5Cl as Solid Electrolyte; *Solid State Ionics* **2013**, *242*, 45–48

[14] Yu, C.; van Eijck, L.; Ganapathy, S.; Wagemaker, M.; Synthesis, Structure and Electrochemical Performance of the Argyrodite Li_6PS_5Cl Solid Slectrolyte for Li-Ion Solid State Batteries; Electrochim. Acta **2016**, 215, 93-99

[15] Richards, W. D.; Miara, L. J.; Wang, Y.; Kim, J. C.; Ceder, G.; Interface Stability in Solid-State Batteries; *Chem. Mater.* **2016**, *28*, 266–273

[16] H. Yokokawa, Thermodynamic stability of sulfide electrolyte/oxide electrode interface in solid-state lithium batteries, *Solid State Ionics* 2016, 285, 126–135.

[17] Zhu, Y.; He, X.; Mo, Y.; Origin of Outstanding Stability in the Lithium Solid Electrolyte Materials: Insights from Thermodynamic Analyses Based on First-Principles Calculations; *ACS Appl. Mater. Interfaces* **2015**, *7*, 23685–23693

[18] Dedryvère, R.; Foix, D.; Franger, S.; Patoux, S.; Daniel, L.; Gonbeau, D.; Electrode/Electrolyte Interface Reactivity in High-Voltage Spinel $LiMn_{1.6}Ni_{0.4}O_4$/$Li_4Ti_5O_{12}$ Lithium-Ion Battery; J. Phys. Chem. C 2010, 114, 10999–11008.

[19] Ji, X.; Lee, K. T.; Nazar, L. F.; A Highly Ordered Nanostructured Carbon-Sulphur Cathode for Lithium-Sulphur Batteries. Nat. Mater. 2009, 8, 500−506.

[20] Vizintin, A.; Lozinšek M.; Chellappan, R. K.; Foix, D.; Krajnc, A.; Mali, G.; Drazic, G.; Genorio, B.; Dedryvère, R.; Dominko, R.; Fluorinated Reduced Graphene Oxide as an Interlayer in Li-S Batteries; Chem. Mater. 2015, 27, 7070-7081.

[21] Franke, R.; Chassé, T.; Streubel, P.; Meisel, A.; Auger Parameters and Relaxation Energies of Phosphorus in Solid Compounds; J. Electron Spectros. Relat. Phenomena 1991, 56, 381–388.

[22] Rödl, T.; Weihrich, R.; Wack, J.; Senker, J.; Pfitzner, A.; Rational Syntheses and Structural Characterization of Sulfur-Rich Phosphorus Polysulfides: α-P_2S_7 and β-P_2S_7; Angew. Chem. Int. Ed. 2011, 50, 10996-11000

[23] A. Sakuda, A. Hayashi, M. Tatsumisago, Interfacial Observation Between $LiCoO_2$ Electrode and Li_2S-P_2S_5 Solid Electrolytes of All-Solid-State Lithium Secondary Batteries Using Transmission Electron Microscopy. *Chem. Mater.* 2010, 22, 949-956.

[24] A. Sakuda, A. Hayashi, T. Ohtomo, S. Hama, M. Tatsumisago, All-Solid-State Lithium Secondary Batteries Using $LiCoO_2$ Particles with Pulsed Laser Deposition Coatings of Li_2S-P_2S_5 Solid Electrolytes. J. Power Sources, 2011, 196, 6735-6741

[25] H. Visbal, Y. Aihara, S. Ito, T. Watanabe, Y. Park, S. Doo, The Effect of Diamond-Like Carbon Coating on $LiNi_{0.8}Co_{0.15}Al_{0.05}O_2$ Particles for All Solid-State Lithium-Ion Batteries Based on Li_2S-P_2S_5 Glass-Ceramics; *J. Power Sources* 2016, 314, 85-92.

[26] M. Tang, V. Sarou-Kanian, P. Melin, J.-B. Leriche, M. Ménétrier, J.-M. Tarascon, M. Deschamps, E. Salager, Following lithiation fronts in paramagnetic electrodes with *in situ* magnetic resonance spectroscopic imaging; *Nat. Commun.* 2016, 7, Article nb. 13284

[27] Wagner, C. D.; Riggs, W. M.; Davis, L. E.; Moulder, J. F.; (G. E. Muilenberg, editor), Perkin-Elmer Corporation (Physical Electronics), Handbook of X-ray photoelectron spectroscopy; 1981.

[28] F. Han , T. Gao , Y. Zhu , K. J. Gaskell, C.; A Battery Made From a Single Material; Wang, *Adv. Mater.* 2015, 27, 3473−3483.

[29] I. Tarhouchi, V. Viallet, P. Vinatier, M. Ménétrier, Electrochemical Characterization of $Li_{10}SnP_2S_{12}$: An Electrolyte or a Negative Electrode for Solid State Li-Ion Batteries?; *Solid State Ionics* 2016, 296, 18-25.